MP-RRT#: a Model Predictive Sampling-based motion planning algorithm for Unmanned Aircraft Systems

International Society for Rock Mechanics and Rock Engineering
Norwegian Group for Rock Mechanics

ISRM International Symposium
Eurock 2025 – Expanding the Underground Space
Trondheim, Norway, 16-20 June
ISBN 978-82-8208-079-8

Mode I fracture toughness of a low-porosity rock subjected to freeze-thaw cycles

G. Torsello
Politecnico di Torino, Torino, Italy
giulia.torsello@polito.it

P. Hamdi & F. Amann
RWTH Aachen University, Aachen, Germany

M. Castelli & R. Bellopede
Politecnico di Torino, Torino, Italy

C. Fidelibus
Università del Salento, Lecce, Italy

Abstract

Rapid climate change significantly impacts periglacial environments, where rising ground temperatures reduce permafrost thickness and expand the active layer. Cyclic Freeze-Thaw (FT) processes within the active layer induce fatigue stress in rock masses. The potential impact on intact rock is primarily influenced by porosity and mineral composition, leading to mechanical degradation of rock bridges, the intact rock areas between discontinuities. Additionally, water cyclic freezing and thawing processes within discontinuities can induce crack tip propagation and the progressive failure of rock bridges, sometimes resulting in rock slope instability. Therefore, understanding the response of intact rock to FT cycles is crucial for permafrost areas, including slope stability assessments in high-altitude mountains.

In this paper, the first phase of an experimental campaign to understand the fatigue behaviour of high-strength, low-porosity fractured rock is reported. The effects of FT cycles on the mechanical properties of a low-porosity quartzite are addressed. Mode I fracture toughness tests are conducted on quartzite Semi-Circular Bend (SCB) specimens with an artificial notch under static loading. The opening of the notch is monitored during the test using a Crack Opening Displacement (COD) gauge, and the development of the Fracture Process Zone (FPZ) above the notch is quantified using the Digital Image Correlation (DIC) technique.

The preliminary results indicate that, unlike high-porosity rocks, the mechanical properties of the high-strength, low-porosity quartzite are not significantly influenced after repeated (60) FT cycles, at temperatures between room temperatures and -12 °C. These findings encourage further research into the effects of cyclic opening-closing due to water-ice transition within natural discontinuities. Moreover, the data provide useful observations for developing a numerical model based on a Fracture Mechanics (FM) approach to study crack behaviour under static and cyclic conditions.

ISRM

NBG

Keywords

Fracture toughness mode I, low-porosity rocks, freeze-thaw cycles, climate change

1 Introduction

In the context of rapid climate change, evaluating rock slope stability is of paramount importance as temperature fluctuations intensify natural weathering processes damaging rock structures. Freeze-Thaw (FT) cycles are among the most significant processes influencing rock stability in cold climates. A seasonal FT cycle happens when, in the cold season, the water infiltrating pores, fissures, and fractures freezes, leading to volumetric expansion during water-ice transition explicatable in frost-heaving forces and then, in the warm season, thaws, modifying the stress regime (Davidson and Nye 1985; Matsuoka 2001). FT cycles can significantly weaken rock masses promoting crack initiation and propagation, particularly in quasi-brittle materials like rocks. Understanding the impact of these cycles is essential for anticipating and managing the potential hazards associated with slope failures, particularly in periglacial environments.

FT cycles occur at diurnal, annual, and millennial scales (Matsuoka et al. 1998). Several factors, including slope aspect, location, elevation, and snow cover condition frequency and intensity. Numerous studies have been conducted to better understand the mechanisms behind FT-induced rockfall events. Research on calcareous cliffs in the French Subalpine Ranges revealed a strong correlation between FT cycles and rockfall events (Frayssines and Hants 2006). A nine-year study of eleven rock sites in the Austrian Alps examined the occurrence of FT cycles, showing that near-surface rocks are the most affected, especially in sun-exposed areas, and snow cover combined with thermal conditions influences the duration of the frost-cracking window (Kellerer-Pirklbauer 2017). These correlations underscore the significance of FT cycles in contributing to slope instability.

Assessing the damage caused by FT cycles is not limited to field observations. In high-porosity rocks, FT cycles reduce compressive and tensile strength, increase porosity, and induce overall deformation, as observed in laboratory experiments. Rock fatigue and damage accumulation under compression occur in sandstones subjected to FT cycles in the laboratory (Jia et al. 2015). Wang et al. (2024) developed a constitutive damaged model for the simulation of the porosity changes, tracked using nuclear magnetic resonance, induced by FT cycles on sandstones under compressive stress. An empirical model for the stress generated along the wall of an open crack by freezing water was defined for limestone by Bost and Pouya (2017); the model is applicable when the structure of the pores is known. The difficulty in determining the pore structure appears to be the main reason behind the challenges in understanding the effects of FT cycles on low-porosity rocks.

This paper is focused on the fracture mechanics response to FT cycles of a low-porosity, fine-grained metamorphic quartzite of the Ambin unit - quartzite of Etache, ascertained by an experimental campaign conceived to address the evolution of the FPZ specifically. The campaign consisted of Semi-Circular Bending (SCB) tests on quartzite specimens in the natural state and after 60 FT cycles, with surface displacements and strains tracked in real-time by using a Digital Image Correlation (DIC) technique. DIC was useful for detailing the strain distribution around the pre-existing notches and capturing microcrack initiation and growth during the loading process, thus offering valuable insights into the evolution of the FPZ. In addition, the micro-aspects of the crack growth paths were analysed by visualizing post-failure thin sections of the specimens. Another target of the experiments is to provide insights into how FT cycles affect the mode I fracture toughness of the quartzite. The findings contribute to understanding how climate change, manifested in a higher severity of the freezing-thawing processes, impacts rock stability and associated risks of rockfalls in mountainous and periglacial regions.

The paper is structured as follows: in Section 2, the properties of the quartzite specimens are described, along with details of the fracture toughness setup and the FT cycles; in Section 3, the results of the experimental tests and their interpretation are presented; finally, in Section 4, some conclusive remarks and comments for a discussion about the behavior of the rock during the experimental campaign are given.

2 Materials and Methods

2.1 Specimen characterization

Etache quartzite blocks were collected at Sommeiller Pass, about 3000 m a.s.l. in the Piedmont Alps, high Susa Valley (NW Italy). Since 2009, the Piedmont Regional Agency for Environmental Protection (ARPA) has established a permafrost monitoring station at Sommeiller Pass as part of the regional network installed during the European project Alpine Space "PermaNet - Permafrost long-term monitoring Network". It consists of three vertical boreholes 5, 10, and 100 m deep respectively, equipped with temperature sensors and a weather station (Coppa et al. 2024).

A series of laboratory tests were carried out to derive the petrophysical and mechanical characteristics of the quartzite. The fine-grained quartzite, with an average grain size of 0.10 mm, is composed of 90% quartz and 10% mica/biotite, determined by X-ray diffraction. Water absorption A_b was measured following EN 13755:2008; apparent density ρ_b, and open porosity p_0 were obtained according to EN 1936:2007. Uniaxial compression strength σ_u, Young modulus E_t, and Poisson ratio ν were estimated on 6 cylinders (diameter D 55 mm, height H 110 mm, H/D 2:1) following ISRM 2018 suggested methods for determining compressive strength and deformability of rock materials. Indirect tensile strength σ_t by Brazilian test was assessed following ISRM 1978 suggested methods for determining the tensile strength of rock materials, on 10 disks (diameter D 55 mm, thickness B 28 mm, D/B 2:1). Mean and standard deviation values of the parameters are listed in Table 1.

Table 1 Mean and standard deviation values of the rock parameters.

A_b [%]	ρ_b [kg/m^3]	p_0 [%]	σ_u [MPa]	E_t [GPa]	ν [-]	σ_t [MPa]
0.3±0.1	2650±15	0.7±0.1	192±55	55±5	0.21	15.2±5

2.2 Mode I fracture toughness

SCB specimens with an artificial notch were prepared following the ISRM 2014 suggested method for determining the static mode I fracture toughness K_{IC}. The blocks were core-drilled using diamond drill bits and sliced into disks, subdivided into semi-circular specimens using a diamond saw. The notches were made using water jet cutting. The values of diameter D, thickness B, crack length a, span distance s, and notch width w of all the specimens are reported in Table 2.

The tests were conducted using a servo-controlled ZwickRoell apparatus equipped with a 100 kN load cell applying a static load P on the specimen at a constant displacement rate of 0.0125 mm/min, thus providing sufficient time for the camera to capture the crack growth. During the tests, the load-line displacement LLD was monitored using LVDTs integrated into the apparatus, while the Crack Opening Displacement (COD) was tracked using an external EPSILON COD gauge. A high-speed camera (Cyclone-25-150 from Optronis) with 1000 frames per second (fps) was used to record the fracture process during the test using digital image correlation (DIC). To improve the contrast of the surface for DIC analysis, random patterns of black speckles were sprayed on the surface of the sample, see Fig. 1. Herein, the following equation is used for K_{IC} (ISRM 2014):

$$K_{IC} = Y' \frac{P_{max}\sqrt{\pi a}}{2RB} \quad (1)$$

where P_{max} is the peak load, and Y' is the mode I dimensionless Stress Intensity Factor (SIF), equal to:

$$Y' = -1.297 + 9.516\frac{s}{2R} - \left(0.47 + 16.457\frac{s}{2R}\right)\beta + \left(1.071 + 34.401\frac{s}{2R}\right)\beta^2 \quad (2)$$

being β equal to a/R.

Table 2 Geometrical characteristics of SCB specimens (in mm).

	value or range (ISRM 2014)	this study
D	larger of 10x grain size or 76	74
B	larger of 0.4D or 30	30
a	$0.4 \le a/R \le 0.6$	16
s	$0.5 \le s/2R \le 0.8$	50
w	$\le 1.5 \pm 0.2$	1±0.05

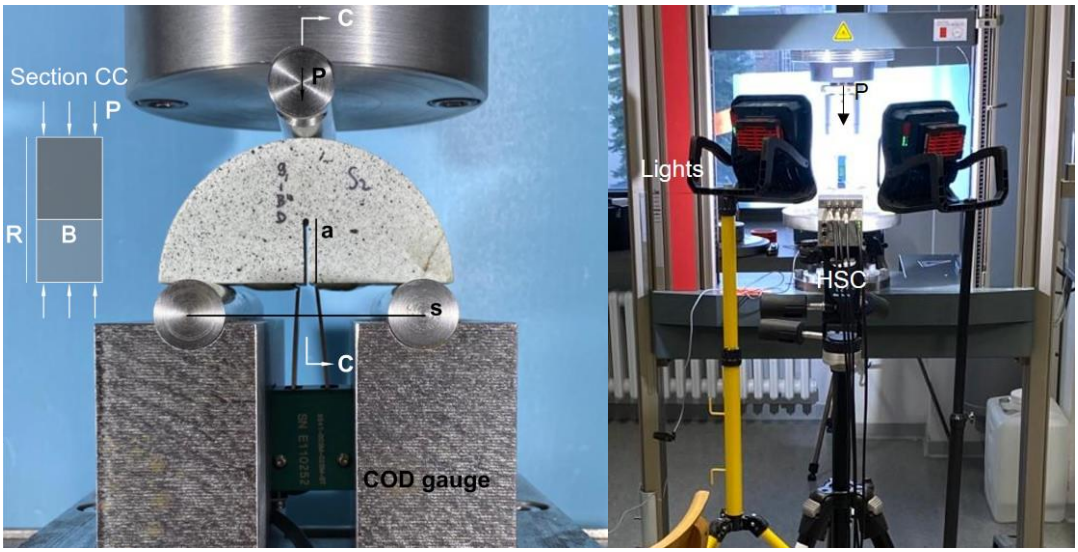

Fig. 1 SCB specimen, loading, and DIC equipment.

2.3 Freeze-thaw cycles

A total of 18 specimens were subjected to SCB tests. 9 *natural* specimens in the first set were tested directly without going through the FT cycles. The remaining *pre-damaged* specimens were later tested after being subjected to 60 FT cycles. The tests were performed in an environmental chamber following EN 12371:2010 (Fig. 2a). Each cycle consisted of 7 hours of freezing in the air at approximately -12°C, followed by 5 hours of thawing in a water bath at room temperature (Fig. 2b) to ensure the superficial saturation of the specimens before the next freezing cycle in air. It is worth noting that the specimens were placed in the environmental chamber without altering their natural state, meaning no forced saturation was applied. Only superficial pore saturation (i.e. open porosity) occurred due to the water in the tank, simulating the natural site conditions on the exposed surfaces of the slope.

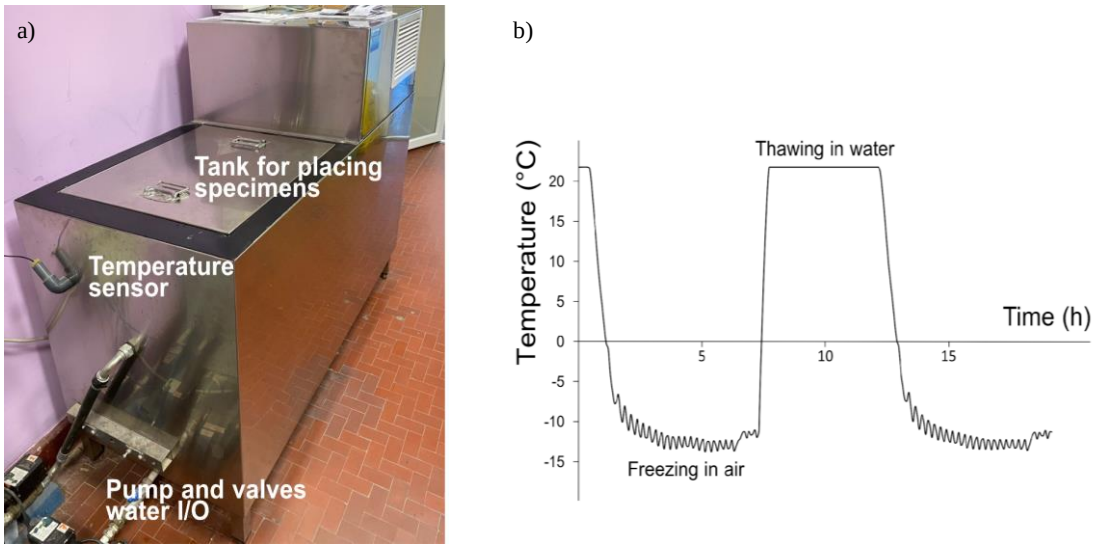

Fig. 2 FT cycles: a) environmental chamber; b) temperatures in the chamber plotted against time for a single cycle.

3 Results and interpretation

Fracture toughness measures the material resistance to crack extension. SIFs, functions of geometry, and boundary conditions represent the stress field around a crack tip. Crack propagation occurs when the SIFs reach a critical value of the fracture toughness (Atkinson 2015). The FPZ around the crack tip is a nonlinear region whose development can be outlined in a load-displacement curve such as the one in Fig. 3. Three stages can be defined (Hoagland et al. 1973): stage I, random cracking upon load application; stage II, tensile microcracking near the notch tip with an elastic response; stage III, increased microcrack growth ahead of the tip, producing a detectable nonlinearity in the curve; stage

IV, microcracks coalescence and formation of a new macrocrack i.e. tension-free crack extending the FPZ in front of the newly created macrocrack.

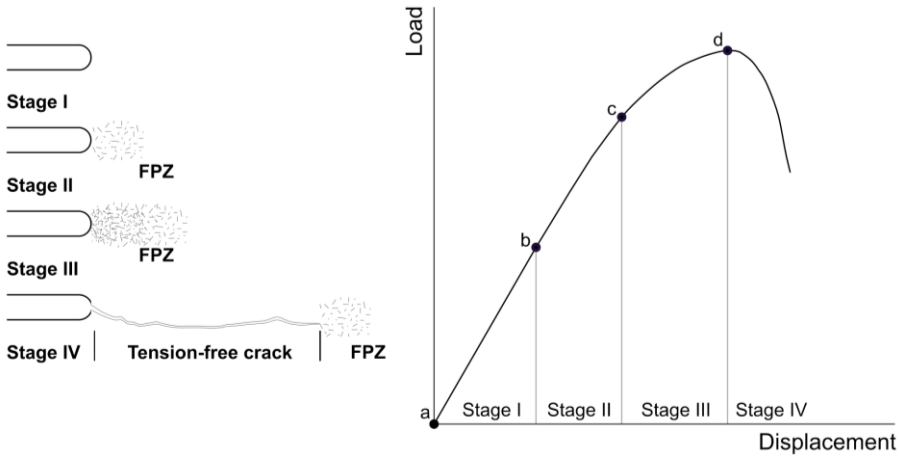

Fig. 3 FPZ development ahead of a crack tip and typical load-displacement curve (modified from Hoagland et al. 1973).

3.1 DIC analysis of the FPZ

In this investigation, the *P*-COD (load vs. crack opening) curves are considered for examining the FPZ development, integrated by the DIC images, providing insights into u_x horizontal displacements and ε_{xx} strains distribution at key loading stages. In Fig. 4a, the curve concerning one of the quartzite specimens is presented, together with the DIC strain maps in Fig. 4c, corresponding to the discrete points *a*-*b* in the curve at 75% and 100% of peak load P_{max}, respectively. In addition, in Fig. 4b the derivative dCOD/d*P* is plotted against *P*. The following statements concerning the four stages can derive from the inspection of these figures:

- Stage I: the linearity in the *P*-COD curve up to point *a* indicates a largely elastic behavior of the quartzite. At this stage, microcracking is minimal, and the FPZ is only starting to form. The DIC strain maps (Fig. 4c, point *a*) support this by showing minor strain and displacement in the horizontal direction, consistent with the steady COD derivative values up to 75% of P_{max} reported in Fig. 4b;

- Stage II and III: transitioning past 75% of P_{max}, the *P*-COD curve deviates from linearity, reflecting the onset of tensile microcracking near the notch tip and FPZ growth. The derivative plot dCOD/d*P* shows a gradual rise as microcracks accumulate. Non-linearity in the *P*-COD curve intensifies around 85% of P_{max} indicating substantial FPZ growth and the derivative drastically changes, reaching a critical value near the peak load P_{max}. The point *b* represents 100 % of P_{max} on the *P*-COD curve and corresponds to K_{IC}. At this stage, the quartzite specimen reaches the maximum load-bearing capacity; beyond this point, the material can no longer withstand additional loading, and the FPZ extends irreversibly (Fig. 4b, point *b*);

- Stage IV is the post-peak behaviour: FPZ reaches maximum expansion, with microcracks coalescing in a macrocrack, leading to complete fracture propagation and specimen failure. After reaching the P_{max}, the testing apparatus is no longer able to record additional load data for the complete post-peak, indicating the material inability to sustain any further stress. However, the DIC camera continued capturing images up to the point of complete specimen failure. In Fig. 5, in the frame captured by the DIC system just before complete failure, the formation of the macrocrack is revealed; the final strain distribution refers to the dynamic transition from microcrack accumulation to macrocrack propagation, with the creation of the tension-free crack. The displacements observed are consistent with the pre-splitting phase, indicating the progression of the fracture before the rock breaks into two parts.

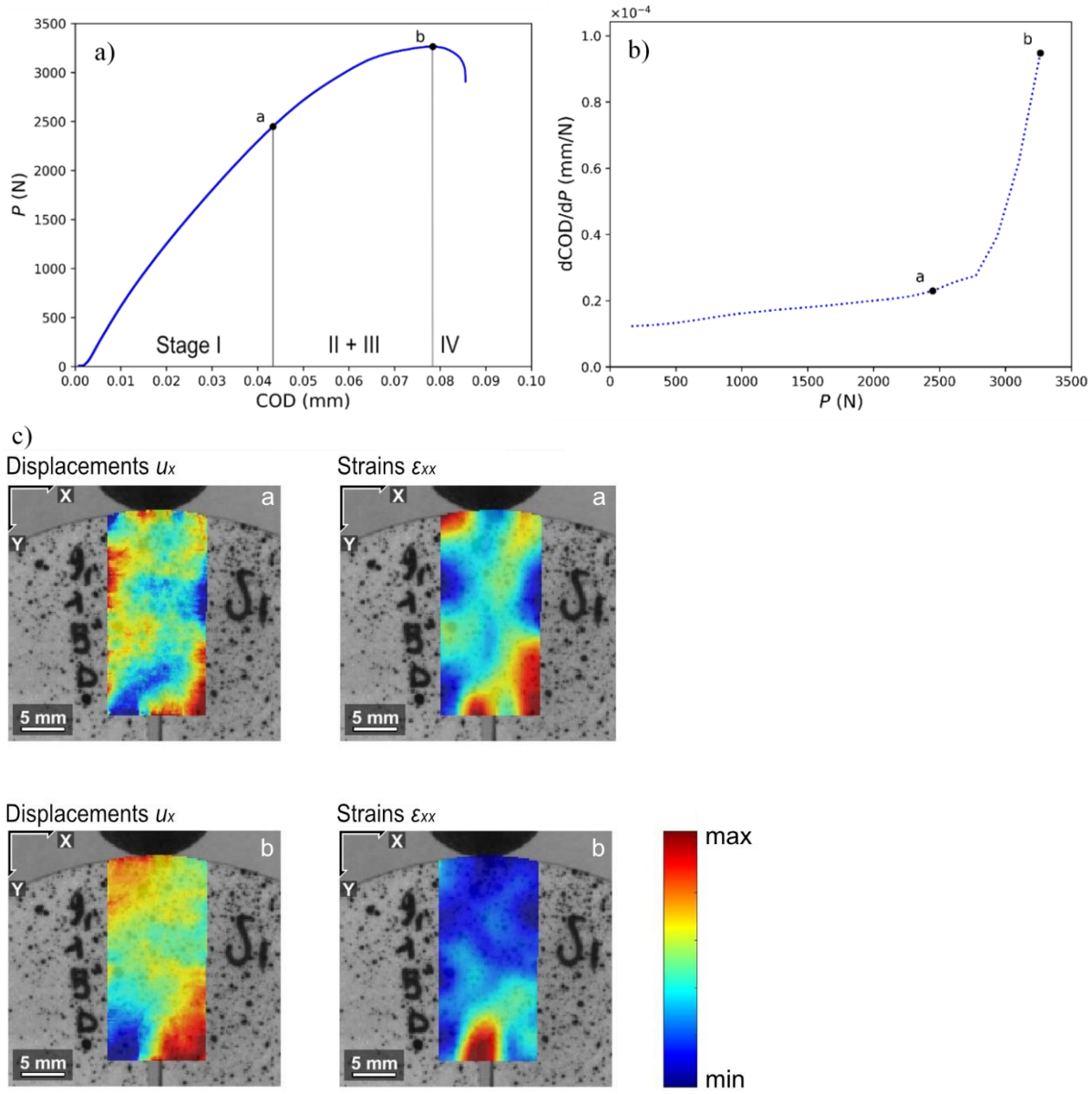

Fig. 4 Load-displacement analysis and DIC results for a quartzite specimen during fracture toughness testing. (a) *P*-COD curve illustrating the different stages of FPZ development; (b) dCOD/d*P* derivative curve highlighting nonlinear responses indicative of FPZ formation; (c) maps of the DIC u_x horizontal displacements and ε_{xx} strains showing the evolution of the fracture from 75% to 100% of peak load, corresponding to points *a*-*b* on the *P*-COD curve.

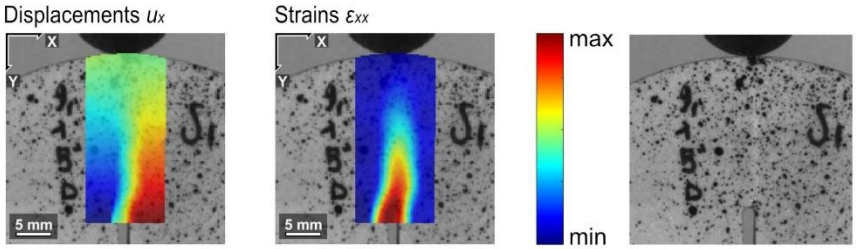

Fig. 5 Tension crack formation and DIC analysis of the final frame before failure, highlighting u_x horizontal displacements and ε_{xx} strains during the development of the tension-free crack.

3.2 Fracture toughness value and load-displacement curves

Following the description of the FPZ development and strain localization using DIC maps, the quantitative results of fracture toughness testing for the quartzite specimens are reported. The DIC analysis provided a visual representation of strain distribution and FPZ formation, however, the ultimate assessment of material resistance to crack propagation is quantified by the fracture toughness parameter K_{IC}. A total of 18 specimens were tested for fracture toughness mode I under static loading

at room temperature, comparing a set of *pre-damaged* specimens after 60 FT cycles and a set of specimens in their *"natural"* state (without FT cycles). The mean, standard deviation, and COV values of P, LLD, and COD at failure, and of K_{IC} (from Eq. 1), for both natural and pre-damaged specimens are summarized in Table 3.

For the natural state specimens, K_{IC} is 1.56 MPa√m ± 0.2 MPa√m, and COV is 14%. P_{max} is 3165 N ± 440 N and COV is 14%. LLD is 0.18 mm ± 0.03 mm, and COV is 15%. For the COD, the mean value is 0.07 mm and the standard deviation is 0.02 mm, while COV is 21%.

After 60 FT cycles, the mean K_{IC} was slightly reduced to 1.54 MPa√m ± 0.2 MPa√m and a COV of 11%. The mean P_{max} was 3125 N ± 390 N and a COV of 12%. The mean LLD remained consistent at 0.18 mm, with a lower standard deviation of 0.02 mm and a COV of 9%. COD mean also remained at 0.07 mm, with a standard deviation of 0.01 mm and a COV of 20%.

Table 3 Mean, standard deviation, and coefficient of variation (COD) of the fracture toughness tests.

		K_{IC} [MPa√m]	P_{max} [N]	LLD [mm]	COD [mm]
Natural	Mean	1.56	3165	0.18	0.07
	Std	0.2	440	0.03	0.02
	COV [%]	14	14	15	21
Pre-damaged	Mean	1.54	3125	0.18	0.07
	Std	0.2	390	0.02	0.01
	COV [%]	11	12	9	20

3.3 Post-failure thin-sections

Post-failure thin sections at the mid-thickness of the specimens were prepared and analysed for 3 specimens in the natural state and 3 specimens subjected to FT cycles. An optical microscope was employed to assess microstructural differences between natural and FT-damaged quartzite specimens and to explore possible explanations for the marginal difference in K_{IC} values. Due to the low porosity of the quartzite under study, the observation of distinct porosity changes from thin sections was precluded. Furthermore, no clear correlation between FT cycling and porosity or microstructural features was evident. Across the 6 thin sections analysed, only minimal differences were identified.

One notable finding was the slight increase in fracture path tortuosity τ, defined as the ratio of the actual fracture path length to the straight-line distance along the path (Chudnovsky & Gorelik 1996). The average value of τ for the undamaged specimens, 1.05, increased slightly to 1.07 for the pre-damaged specimens. This slight increase in tortuosity may reflect minor microstructural changes and may influence the crack propagation paths.

Additionally, the fracture analysis revealed a modest increase in intragranular fracture percentage in the pre-damaged specimens compared to the natural ones. In natural specimens, 21% of the fracture surfaces were intragranular, while in damaged samples the percentage was 26%, indicating that FT cycles may have slightly weakened grains, resulting in a higher tendency for fractures to propagate through grains rather than along grain boundaries.

4 Discussion and conclusion

This paper investigates the fracture toughness of a low-porosity quartzite (with less than 1% open porosity) after exposure to 60 FT cycles, focusing on mode I (opening) fracture toughness of SCB quartzite specimens. Specimens were tested both in their natural state and after undergoing 60 FT cycles between -12°C and room temperature, with additional analysis of the FPZ through high-speed camera DIC imaging and post-failure thin-sections.

The experimental findings indicate that FPZ formation in quartzite remains elastically stable up to approximately 75% of the peak load, showing minimal deformation. However, as the load approaches peak levels, strain around the notch tip increases significantly, leading to unstable crack growth and dynamic failure. This process corresponds to the nonlinear behaviour observed in the COD measurements. The mean value of the fracture toughness K_{IC} is 1.56 MPa√m for natural specimens, slightly more than 1.54 MPa√m for the specimens subjected to FT cycles. The corresponding minimal damage ratio is 1.3%, suggesting that the performed 60 FT cycles have a negligible effect on the

fracture resistance of this low-porosity quartzite. Post-failure thin-section analysis further supported these findings, showing only minor microstructural differences between natural and FT pre-damaged specimens. Observations of slightly increased tortuosity and a modest rise in intragranular fracture in damaged specimens imply that FT cycles may induce minor microstructural changes. However, these alterations were insufficient to impact fracture toughness values noticeably.

The insights gained from this study emphasize the importance of porosity in determining intact rock vulnerability to FT damage. Future research will expand this investigation by examining high-porosity rocks under FT cycles to explore potential correlations between porosity, microstructural damage, and fracture toughness. The next phase of this research will be aimed at assessing whether the frost-heaving force generated by water-ice expansion within larger-scale discontinuities could lead to significant damage (Matsuoka 1990). Specifically, it is to investigate if repeated FT cycles in fractures and joints may induce fatigue damage at the crack tip.

Acknowledgments

This study was carried out within the RETURN Extended Partnership and received funding from the European Union Next-GenerationEU (National Recovery and Resilience Plan – NRRP, Mission 4, Component 2, Investment 1.3 – D.D. 1243 2/8/2022, PE0000005) – SPOKE VS 2.

References

Davidson G. P., and Nye J. F. (1985) A photoelastic study of ice pressure in rock cracks. Cold Regions Science and Technology 11.2:141-153.

Matsuoka N. (2001) Microgelivation versus macrogelivation: towards bridging the gap between laboratory and field frost weathering. Permafrost and Periglacial Processes 12.3:299-313.

Matsuoka N., Hirakawa K., Watanabe T., Haeberli W., and Keller F. (1998) The role of diurnal, annual and millennial freeze-thaw cycles in controlling alpine slope instability. In Proceedings of the Seventh International Conference on Permafrost. Centre d'Etudes Nordiques, Universite Laval.

Frayssines M. and Hants D. (2006) Failure mechanisms and triggering factors in calcareous cliffs of the subalpine ranges (French Alps). Engineering Geology 86(4):256–270.

Kellerer-Pirklbauer A. (2017) Potential weathering by freeze-thaw action in alpine rocks in the European Alps during a nine-year monitoring period. Geomorphology 296:113–131, 2017.

Jia H., Xiang W., and Krautblatter M. (2015) Quantifying rock fatigue and decreasing compressive and tensile strength after repeated freeze-thaw cycles. Permafrost and Periglacial Processes 26(4):368–377.

Wang Z., Yu, M., Wang, L., Xie H., Xu Y., and Wang L. (2024) Strength degradation characteristics and damage constitutive model of sandstone under freeze-thaw cycles. Scientific Reports 14:22674.

Bost M., Pouya A. (2017). Stress generated by the freeze-thaw process in open cracks of rock walls: empirical model for tight limestone. Bulletin of Engineering Geology and the Environment 76(4):1491-1505.

Coppa G., Sanna F., Paro, L., Musacchio C., and Merlone, A. (2024) Metrological approach for permafrost temperature measurements. Cold Regions Science and Technology 229:104364.

Atkinson B. K. (Ed. 2015) Fracture Mechanics of Rock. Elsevier.

Hoagland R. G., Hahn G. T. and Rosenfield A. R. (1973). Influence of microstructure on fracture propagation in rock. Rock Mechanics 5(2):77–106.

Chudnovsky A. and Gorelik, M. (1996). Tortuosity of crack path, fracture toughness and scale effect in brittle fracture. Size-scale effects in the failure mechanisms of materials and structures, 97-108.

Matsuoka N. (1990). Mechanisms of rock breakdown by frost action: an experimental approach. Cold Regions Science and Technology 17(3): 253-270.